



ELSEVIER

Polymer 43 (2002) 5321–5328

polymerwww.elsevier.com/locate/polymer

Solid-state morphologies of linear and bottlebrush-shaped polystyrene–poly(Z-L-lysine) block copolymers

Helmut Schlaad^{a,*}, Hildegard Kukula^a, Bernd Smarsly^a, Markus Antonietti^a, Tadeusz Pakula^b^aMax-Planck-Institut für Kolloid- und Grenzflächenforschung, Abteilung Kolloidchemie, Am Mühlenberg 1, D-14476 Golm, Germany^bMax-Planck-Institut für Polymerforschung, Ackermannweg 10, D-55128 Mainz, Germany

Received 26 March 2002; received in revised form 3 May 2002; accepted 5 June 2002

Abstract

The solid-state structures of polystyrene–poly(Z-L-lysine) block copolymers were examined with respect to the polymer architecture and the secondary structure of the polypeptide using circular dichroism, quantitative small- and wide-angle X-ray scattering, and electron microscopy. Linear block copolymers exhibit a *hexagonal-in-lamellar* structure where folded and packed polypeptide α -helices form lamellae which extend over an exceptional broad range of the composition diagram. Star- or bottlebrush-shaped copolymers are able to stabilize a larger interface area than linear ones which promotes the formation of undulated lamellar mesophases. Depending on the secondary structure of polypeptide segments, plane lamellar, superundulated lamellar, or corrugated lamellar phases are formed. These results indicate the importance of a secondary structure and packing of polymer chains for the formation of new phases and ordering far from the ‘classical’ phase behavior. © 2002 Elsevier Science Ltd. All rights reserved.

Keywords: Polypeptide block copolymer; Polymer architecture; Solid-state morphology

1. Introduction

In recent years, the formation of block copolymer mesophases has become a model case to examine the self-assembly of macromolecular systems [1–4]. Up to now, the majority of analyzed systems deal with block copolymers having similar cohesion energies where both blocks can adopt a flexible or semi-flexible conformation. The resulting spherical, cylindrical, gyroid, lamellar, and other phases could thus be explained by the counterbalance of elastic energy and thermodynamic demixing [3,4].

For the generation of novel phases and physical effects, additional energy contributions must be included in this delicate energy balance. The employment of more immiscible monomer pairs, as it was done with partially fluorinated block copolymers [5], adds interface energy as a relevant parameter and new stable phases, all from the lamellar phase family, were found.

Another approach is the employment of rigid polymer units, referred to as rod–coil block copolymers [6,7]. Here,

liquid crystalline order and packing energy contributions lead to deviations from the phase behavior of conformationally isotropic block copolymers. First introduced by François et al. [8–11] Thomas et al. [12,13] examined the phase behavior of rod–coil polymers in a more systematic fashion. Besides revealing a multiplicity of new and exciting structures, such as an ordered zigzag phase, these authors also highlighted the problems of metastability of such phases. However, rigidity remarkably slows down exchange dynamics, and thus the regularity of structures will delicately depend on the synthesis protocol.

A very interesting class of rod–coil block copolymers are made of a synthetic (e.g. polystyrene or polybutadiene) and an α -helical polypeptide segment (e.g. poly(γ -benzyl-L-glutamate) or poly(N^{ϵ} -benzyloxycarbonyl (Z)-L-lysine)). Since such ‘hybrid’ or ‘chimera’ polymers are well known for about 25 years (for a review, see Refs. [14,15]), their chemistry is not particularly new. Gallot et al. [16–21] examined the solid-state structure of those block copolymers and found a remarkable preference of lamellar phases independent of the composition, with the peptide α -helices generally folded and tightly packed in plane (cf. Chart 1(A)). However, the finer structural details could not be elucidated since various data manipulation methods only became available at a later stage.

* Corresponding author. Tel.: +49-331-567-9514; fax: +49-331-567-9502.

E-mail address: schlaad@mpikg-golm.mpg.de (H. Schlaad).

¹ <http://www.mpikg-golm.mpg.de/kc/>

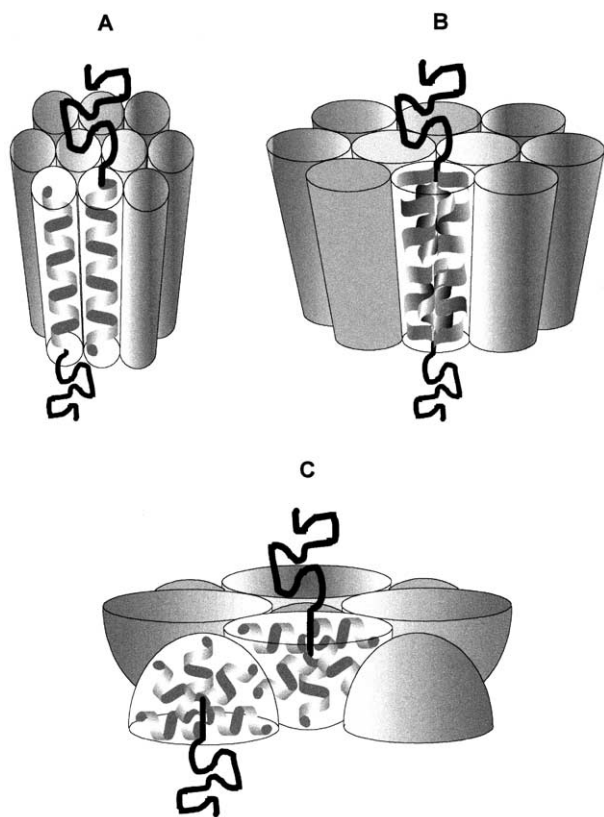


Chart 1. Schematic representation of the superstructures triggered by different architectures of polyvinyl-polypeptide block copolymers. (A) linear copolymers (adopted from Ref. [19]), (B) and (C) star- or bottlebrush-shaped copolymers.

In the present paper, we want to analyze the solid-state phase structure of hybrid block copolymers of polystyrene and poly(*Z*-L-lysine) with respect to a number of parameters, in particular the polymer architecture and the secondary structure of the polypeptide. In a first set of experiments, we examined three linear block copolymer samples with small-angle X-ray scattering (SAXS). This data was evaluated by means of a method that makes use of the interface-curvature algorithm [22]. In a second set, we investigated multiarm star block copolymers, which were prepared by grafting from ω -multifunctional polystyrene initiators, with one linear polystyrene segment and a polypeptide bottlebrush block (see Chart 1). Here, whether or not the polypeptide takes an helical conformation will depend on the length of the individual bottlebrush arm and not on the total number of peptide repeating units. When the polypeptide segments are too short and are in a non-helical conformation, the bottlebrush units can form by themselves quite stiff cylinders [23–25] which have a much larger diameter than an α -helix (cf. Chart 1(B)); the packing of those cylinders is then expected to give an additional energy contribution and affect structure formation. Finally, when the polypeptide grafts on the bottlebrush are long enough to adopt an α -helical secondary structure, the most compli-

cated geometry of the bottlebrush unit is realized, as is illustrated in Chart 1(C).

We have to mention that this is only one part of a more general scheme how the combination of primary structure (\equiv chain sequence) and secondary structure (\equiv chain folding and helix formation) can influence the formation of superstructures of synthetic polymers. Obviously, this approach borrows some basic elements from biological patterns, but so far synthetic polymer chemists have barely made use of it. However, secondary structure-effects should extend the possibilities to control the self-assembly of polymers.

2. Experimental section

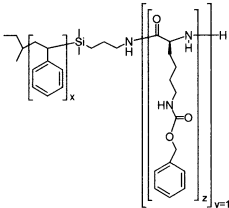
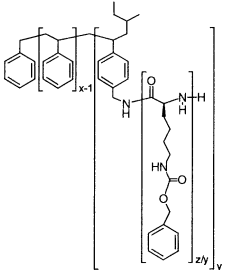
Block copolymer synthesis and characterization. Block copolymer samples were prepared by the ring-opening polymerization of *Z*-L-lysine-*N*-carboxyanhydride (NCA) initiated by ω -amino-functional polystyrenes (amino functionality, $y = 1, 4, 8,$ and 12). The general procedure for the synthesis of macroinitiators and polypeptide block copolymers as well as their characterization have been reported elsewhere [16–21,26,27]. The architecture of the resulting copolymer is determined by the amino functionality of the used macroinitiator: linear copolymers are obtained when $y = 1$ (\rightarrow L1, L2, and L3; see Table 1) and bottlebrush-shaped ones when $y = 4$ (\rightarrow S1), 8 (\rightarrow S2 and S3), and 12 (\rightarrow S4, S5, and S6). As indicated by SEC (eluent: *N,N*-dimethylacetamide + 0.5 wt% LiBr at 70 °C, flow rate: 1 ml/min, columns: 300 \times 8 mm, 10 μ m PSS-GRAM polyester gel: 30, 30, 100, 3000 Å, detectors: UV and RI), the copolymer samples were free of homopolymer impurities and exhibited monomodal molecular weight distributions (except for S1 and S3 that exhibited a bimodal chromatogram) with apparent polydispersity indices of 1.2–1.4 (SEC, polystyrene calibration). The molecular characteristics of the copolymer samples are summarized in Table 1.

Preparation of polymer films. Polymer films of ~ 1 mm thickness were prepared by solvent-casting from 5–10 wt% polymer solutions in *N,N*-dimethylformamide (DMF) as a non-selective solvent; liquid samples on teflon-coated aluminum foil (BYTAC[®]) were slowly dried within 12–24 h at 40 °C. (In order to investigate the effect of casting conditions, additional specimens were prepared from chloroform or dioxane and/or were annealed at 110 °C above the glass transition temperature of polystyrene.)

Structural analysis of block copolymers. Circular dichroism (CD) spectra were recorded with a Jasco J 715 on thin block copolymer films; specimens were prepared from 20 wt% polymer solutions in DMF by spin-coating on a quartz plate. SAXS curves were recorded by means of a Kratky camera and rotating anode instruments with pinhole collimation at room temperature. A Nonius rotating anode (4 kW, Cu K_{α}) and an image-plate detector system were used with respect to the pinhole system. With the image plates

Table 1

Chemical structures and molecular characteristics of the investigated linear (L1–L3) and bottlebrush-shaped (S1–S6) polystyrene-*block*-poly(Z-L-lysine) copolymer samples

Copolymer sample	f_L	x	z	y	z/y	M_n (g/mol)	Φ_L	
	L1	0.57	52	69	1	69	23,700	0.74
	L2	0.68	52	111	1	111	34,700	0.82
	L3	0.30	218	93	1	93	47,200	0.48
	S1	0.57	182	243	4	61	83,200	0.74
	S2	0.25	193	65	8	8	38,200	0.41
	S3	0.57	193	255	8	32	88,000	0.73
	S4	0.22	188	54	12	5	35,400	0.37
	S5	0.40	188	123	12	10	53,400	0.57
	S6	0.55	188	227	12	19	80,700	0.71

f_L : mole fraction of Z-L-lysine in the copolymer (NMR). x , z : average number of styrene and Z-L-lysine repeating units, respectively, (SEC, NMR). y : number of polypeptide segments per polymer molecule (= amino functionality of the macroinitiator; MALDI-TOF MS). z/y : number of Z-L-lysine repeating units per segment. M_n : number-average molecular weight of the copolymer. Φ_L : volume fraction of Z-L-lysine, $\Phi_L = 1 - \Phi_S = 1/[1 + (M_S \rho_L / M_L \rho_S)]$, M_S , M_L : molar mass of styrene and Z-L-lysine, ρ_L , ρ_S : specific densities of polystyrene (1.0901 g/ml) and poly(Z-L-lysine) (1.2645 g/ml), determined in DMF at +40 °C.

placed at a distance of 40 cm from the sample, a scattering vector range from $s = 2/\lambda \sin \theta = 0.05 - 1.6 \text{ nm}^{-1}$ (2θ : scattering angle, $\lambda = 0.15418 \text{ nm}$) was available. Further analyses were performed using a Rigaku rotating anode (18 kW, Cu K_α) X-ray beam with a pinhole collimation and a two-dimensional detector (Bruker) with 1024×1024 pixels was used. The beam diameter was about 0.5 mm and the sample to detector distance was 1.3 m. 2D diffraction patterns were transformed into a 1D radial average of the scattering intensity. For the Kratky camera (slit collimation), a proportional counter (Anton Paar, Graz, Austria) was used, thus recording scattering data in the range of $s = 0.03 - 0.95 \text{ nm}^{-1}$.

Transmission electron microscopic (TEM) analyses were performed with a Zeiss EM 912 Omega operating at 120 kV. Polymer films having a thickness of 30–50 nm were prepared with an ultramicrotome Leica Ultracut UCT and were transferred onto carbon-coated copper grids. For a selective staining of poly(Z-L-lysine), specimens were exposed to the vapor of a freshly prepared aqueous RuO_4 solution for 1–3 min.

3. Results and discussion

3.1. Linear polypeptide block copolymers

Gallot et al. [16–21] investigated the solid-state

morphologies of linear polyvinyl–polypeptide coil–rod block copolymers by SAXS. They found, regardless of the volume fraction of the two comonomers, a lamellar morphology of alternating polyvinyl and polypeptide sheets. The intersheet spacing or long period (d) was determined to be 25–35 nm depending on the molecular weight of the copolymer. In addition to this lamellar superstructure, the α -helical polypeptide chains were arranged in a hexagonal array with a characteristic spacing of $d_H = 1.5 \text{ nm}$ and were generally folded. Hence, these block copolymers form a *hexagonal-in-lamellar* morphology as depicted in Chart 1(A), and their phase behavior is vastly different from that of conformationally isotropic diblock copolymers [3,4].

For the direct comparison of published results with our studies on the morphology of bottlebrush-shaped polystyrene-*block*-poly(Z-L-lysine)_s, and to establish our numerical procedures, we first investigated the films of three linear copolymers with different molecular weights and chemical compositions (L1–L3; see Table 1) by CD and SAXS. The CD spectrum of any polymer film shows the characteristic curve of a polypeptide α -helix (cf. Fig. 1(A)) [28], thus confirming the coil–rod conformation of the block copolymers. The SAXS patterns at higher scattering vectors ($s > 0.6 \text{ nm}^{-1}$; cf. Fig. 1(B)) show a set of three lines with Bragg spacings in the ratio $1 : \sqrt{3} : 2$ which arise from the hexagonal array of α -helices with a distance of

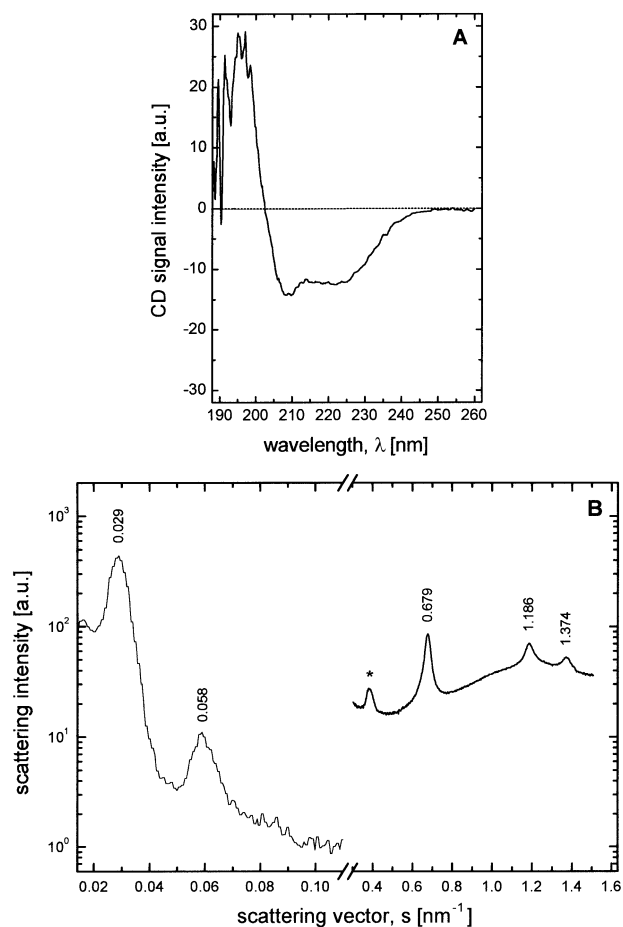


Fig. 1. Exemplary CD spectrum (A) and radial-averaged SAXS curve (B; parallel alignment of the specimen to the X-ray beam, cf. Fig. 6 of the polymer film L3. The peak denoted with * ($s = 0.386 \text{ nm}^{-1}$) was only observed for L3 and could not be assigned yet.

$d_H \approx 1.5 \text{ nm}$. Using the Scherrer equation [29,30], we can calculate a correlation length of 20 nm from the width of the peaks. From volume calculations this translates to approximately 150 helices within an ordered domain; this indicates a high packing energy and packing order within the polypeptide mesophases. At lower scattering vectors ($s < 0.1 \text{ nm}^{-1}$), two peaks were usually observed with a spacing ratio of 1:2 which is characteristic of a lamellar morphology. The intersheet spacing is $d = 16.6, 29.4,$ and 34.5 nm for the three investigated polymer films L1–L3,

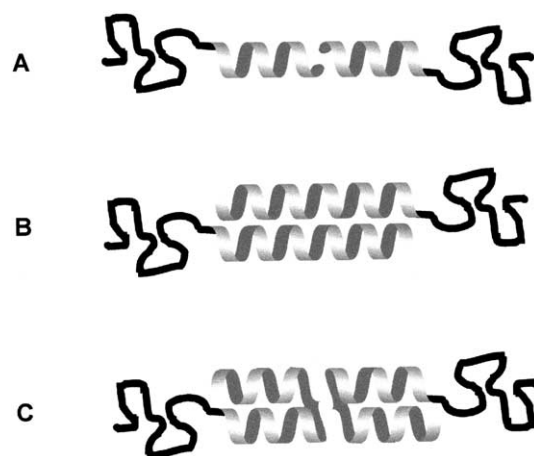


Chart 2. Illustration of the possible arrangements of polypeptide helices. (A) stacking, (B) interdigitation, (C) folding.

i.e. the dimension of the sheets increases with increasing molecular weight of the copolymer (see Table 2). Hence, our studies confirm the *hexagonal-in-lamellar* morphology of linear polystyrene–poly(Z-L-lysine) block copolymers as it was proposed by Douy and Gallot [16–21]. However, these authors reported even higher than second-order Bragg peaks at very low scattering angles which indicates a higher ordering of lamellae in these films. This can be explained by a very slow exchange dynamics within such films which makes a long-range ordering dependent on casting conditions.

Since all structures show lamellar morphology with a long-range hexagonal packing within the plane, it is possible to gain some information on the conformation of a single block copolymer chain. Dividing the molecular volume by the average lateral extension of a chain ($= d/2$) (\rightarrow interface area per chain) and the cross-section of a helix ($= d_H^2 \pi/4$) yields a parameter γ that specifies stacking, interdigitation or folding of the helices. As illustrated in Chart 2, stacked helices give $\gamma = 1$ whereas interdigitated or once-folded helices reveal two unit areas per chain or $\gamma = 2$. A value of $\gamma > 2$ is indicative of two or more times folded helices. It is seen from the data in Table 2, that the γ values for the three linear block copolymers are between 1.9 and 2.6. This would indicate that the helices are not stacked but are rather interdigitated or rarely folded (cf. Ref. [19]). It is worth mentioning that the maximum length of the

Table 2

Characteristics of the solid-state lamellar morphologies of the linear polystyrene–poly(Z-L-lysine) block copolymers L1–L3 (DMF-cast polymer films)

Sample	l_H (nm)	d_H (nm)	d (nm)	d_S (nm)	d_L (nm)	$d_S + d_L$ (nm)	$\kappa; \iota$	γ	Morphology
L1	10.3	1.42	16.6	4.5	12.2	16.7	1.2;2.0	2.6	Hexagonal-in-lamellar
L2	16.6	1.49	29.4	4.8	21.7	26.5	1.9;2.2	1.9	Hexagonal-in-lamellar
L3	13.9	1.48	34.5	13.8	12.7	26.5	1.4;2.0	2.4	Hexagonal-in-lamellar

l_H : maximum length of an poly(Z-L-lysine) α -helix, $l_H = 1.5z \text{ \AA}$, calculated according to Ref. [19]. d_H : spacing between helices (SAXS). d : intersheet spacing (SAXS). d_S, d_L : dimension of polystyrene and poly(Z-L-lysine) sheets, respectively, calculated according to Ref. [31]. κ, ι : normalized scattering average of curvature and interface area, respectively, determined according to Ref. [22]. γ : geometrical factor, $\gamma = (8 \times 10^{21} / \pi N_A)(M_n / \rho d d_H^2)$, N_A : Avogadro constant, ρ : specific density of the copolymer (L1: 1.1714 g/ml, L2: 1.2033 g/ml, L3: 1.1004 g/ml).

α -helices (l_H) is comparable to the thickness of poly(Z-L-lysine) layers (d_L ; see Table 2), which further excludes the possibility of stacking. Since polypeptide α -helices produce a strong electric dipole moment along the molecule axis, both interdigitation and helix folding are ways to minimize the energy of the superstructure of helices.

The SAXS data can be further evaluated by means of the concept of the ‘interface distribution function’ introduced by Ruland [31]. This method allows for the determination of the relative thickness of the polystyrene (d_S) and poly(Z-L-lysine) subphase (d_L) from the shape of scattering peaks (for details, see Ref. [31]). These values are listed in Table 2 together with the sum ($d_S + d_L$), which is a second measure of the long period d . However, these values deviate in a systematic fashion from the ones obtained from the position of the peak maximum applying Bragg’s law. This is a first indication to the possible existence of fluctuations or undulations along the lamellae which are neither considered by the Bragg equation nor by simple calculations of the interface correlation function.

In order to gain more information about the structural details, the data were also analyzed in terms of the curvature-interface formalism [22]. Within this formalism, an averaged normalized interface area (ι , ν) and a normalized scattering-average of curvature (κ , κ) are calculated from the shape of the scattering peak via the so-called characteristic function (for details, see Ref. [22]). The advantage of this technique is that it allows the assignment of phases even in absence of long-range order. It is based on the local interface and curvature properties, which are assumed to equilibrate rather fast and—to our experience—do not rely on the preparation path. The κ – ν data are summarized in Table 2 and are also printed in Fig. 4 in a so-called generalized phase diagram. It shows that all data are located on the line of undulated lamellae, although the sample L2 (Fig. 4: square at the furthest right) could also adopt a hexagonal phase which would possess a similar curvature but lower interface energy. This demonstrates that coil–rod block copolymers generate a lamellar morphology when the gain of cohesion energy from the parallel packing of helices is higher than the loss in interface energy. The fact that the phases show the high surface area of lamellar structures but possess curvature indicates the existence of pronounced undulations [12,13,33–36].

3.2. Bottlebrush-shaped polypeptide block copolymers

In the case of the bottlebrush-shaped block copolymers S1–S6, only the peptide segments of S1, S3, and S6 with at least 19 lysine repeating units (z/y ; see Table 1) were found in an α -helical conformation (CD; Fig. 2(A)). This is due to the fact that the formation of a helix usually requires a minimum of 10 amino acid units (S2, S4, S5: $z/y = 5$ –10) [32]. Hence, only the films of S1, S3, and S6 might at all show the characteristic Bragg peaks of a hexagonal packing of α -helices. Such a structure with $d_H \approx 1.4$ nm was indeed

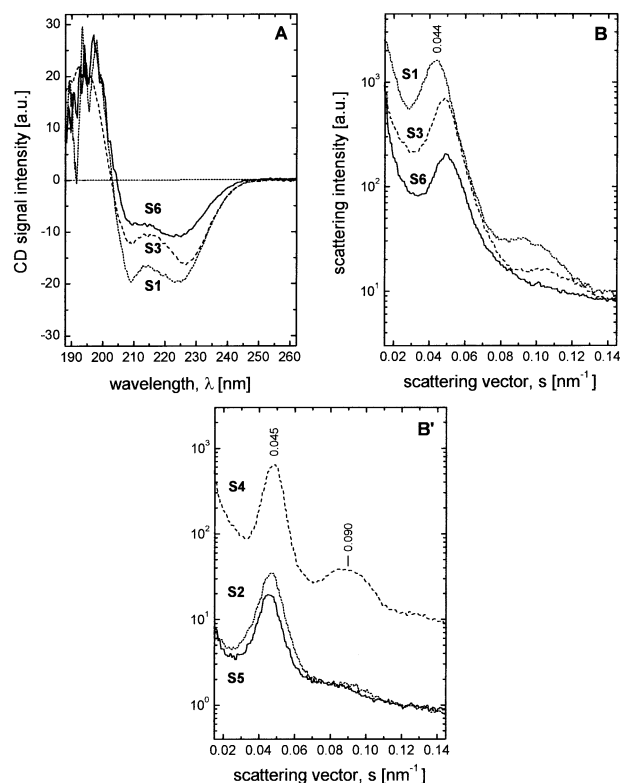


Fig. 2. CD spectra (A) and radial-averaged SAXS curves (B; orthogonal alignment of specimens to the X-ray beam, cf. Fig. 6 of S1–S6. Note that the measured CD signal intensity is not a direct measure of the helix content as it also depends on the chain length of the polypeptide [28] (and the thickness of the film).

found for the first two samples with 61 (S1) and 32 (S3) Z-L-lysine units per segment but not for S6 ($z/y = 19$) (SAXS). This observation underlines the earlier discussed hindrance of helix formation due to the steric overcrowding along the bottlebrush backbone. The correlation length was determined to be 9–11 nm in the isotropically averaged state corresponding to six helices in a line. These specimens are thus in a less ordered state than the ones prepared from linear copolymers with a correlation length of 20 nm (see above). This is also reflected by the broad SAXS peaks in the low-angle region, and the fact that only S4 shows at all a second-order Bragg peak (see Fig. 2(B)) which allows the clear identification of a lamellar phase. It should be noted that the ordering in the films was not affected upon varying the casting conditions (cf. Section 2).

We can attribute a long period to all six polymers which is rather independent of molecular weight and relative volume fractions: $d \approx 21$ nm (see Table 3 and Fig. 3). Obviously, the dense branching of bottlebrushes leads to significantly smaller repeat periods as compared to linear chains even though the overall molecular weights are much higher. This can be explained by a parallel arrangement of the grafted polypeptide chains to the interface, as illustrated in Chart 1(B) and (C). Hence, the bottlebrushes are stabilizing a larger interface area (cf. Refs. [26,27]) but do

Table 3

Characteristics of the solid-state lamellar morphologies of the bottlebrush-shaped polystyrene–poly(Z-L-lysine) block copolymers **S1–S6** (DMF-cast polymer films)

Sample	l_H (nm)	d_H (nm)	d (nm)	d_S (nm)	d_L (nm)	$d_S + d_L$ (nm)	$\kappa; \iota$	Morphology
S1	9.2	1.43	22.9	6.2	17.5	23.7	1.2;2.0	Undulated lamellar
S2	–	–	21.3	8.8	12.7	21.5	1.3;2.1	Undulated lamellar
S3	4.8	1.41	20.6	5.7	15.5	21.2	1.6;2.7	Undulated lamellar
S4	–	–	17.0	–	–	–	1.6;2.1	Undulated lamellar
S5	–	–	22.0	6.7	8.9	15.6	1.3;3.0	Undulated lamellar
S6	2.9	– ^a	20.4	6.5	16.0	22.5	0.3;2.0	Plane lamellar

cf. Table 2.

^a No hexagonal packing (SAXS) despite of an α -helical conformation of polypeptide segments (CD).

only weakly contribute to the thickness of the microdomain (d_L). For this situation, simple geometric considerations result in the following scaling law for the dependence of the long period on the number of monomers in each unit: $d = d_S x^1 + d_L y^0$. Comparison of the absolute thickness of phases (see Table 3) with the contour length of the bottlebrush backbone (1–2 nm) reveals that the bottlebrushes themselves should be stacked from both sides or form a ‘cap’ as illustrated in Chart 1(B) and (C), respectively.

Analysis with the κ – ι formalism reveals a plane lamellar structure for **S6**, whereas undulated and curved structures were found for **S1–S5** (see Table 3 and Fig. 4). In case of **S3** and **S5** (Fig. 4: circles at the furthest top), scattering peaks are broad but the quantitative evaluation [33,34] reveals an excess area of 35 and 50%, respectively, which speaks for ‘superundulated’ lamellar phases. Note that such structures were also reported for polyelectrolyte–lipid complexes [33, 34] or polystyrene–polyisocyanate block copolymers (disordered zigzag phase) [12,13]. However, the experimental interface distribution curves $g_1(r)$ (r = chord length, see

Refs. [37–39]) for all samples can be fitted to a model that takes into consideration that the stacks are extended ‘infinitely’ but the thickness of the individual lamellae is fluctuating (cf. Fig. 5). This means that the lamellar structure should be—despite of the ill-structured SAXS patterns—well developed which indeed could be visualized for **S4** by TEM (see Fig. 7). The lamellae are thus rather rigid to pack well but the thickness of layers is varying or fluctuating which can be explained by the high excess area and entropic forces (so-called packing frustrations).

The bottlebrush-shaped copolymer **S4**, which has the lowest content of Z-L-lysine ($\Phi_L = 0.37$) but highest degree of branching ($y = 12$), forms highly ordered films by simple solvent casting. Furthermore, additional macroscopically anisotropic scattering features are evident as indicated by the 2D-SAXS patterns in Fig. 6. Film alignment perpendicular to the X-ray beam leads to the observation of equidistant, centro-symmetric rings (Fig. 6(A)), whereas a distorted hexagonal pattern is found for a parallel orientation (Fig. 6(B)). These two patterns as well as the κ – ι data

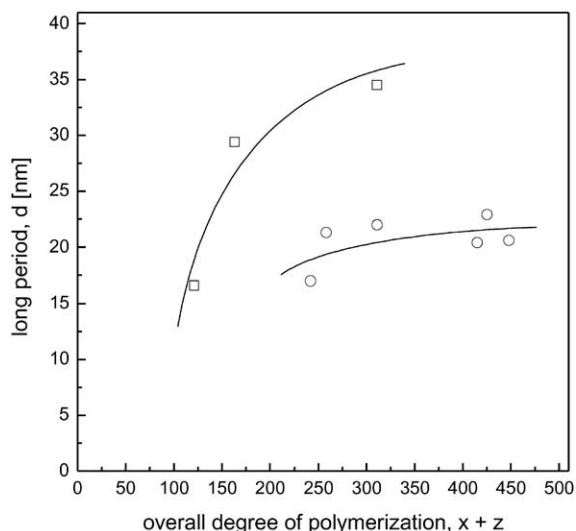


Fig. 3. Dependence of the long period d on the total degree of polymerization ($x + z$) of the linear (\square) and bottlebrush-shaped (\circ) polystyrene–poly(Z-L-lysine) block copolymers (lines are just for guiding the eye).

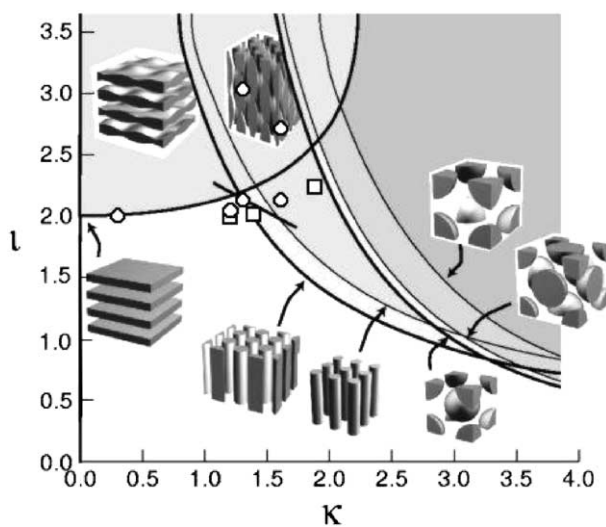


Fig. 4. Experimental κ – ι data, inserted in the generalized phase diagram adopted from Ref. [22] (gyroid phase omitted). \square : linear block copolymers; \circ : bottlebrush-shaped block copolymers. Note that most samples are placed along the line of undulated lamellae, whereas **S3** and **S5** are more in the lamellar region, indicating some high surface area lamellar modifications such as zigzag phases.

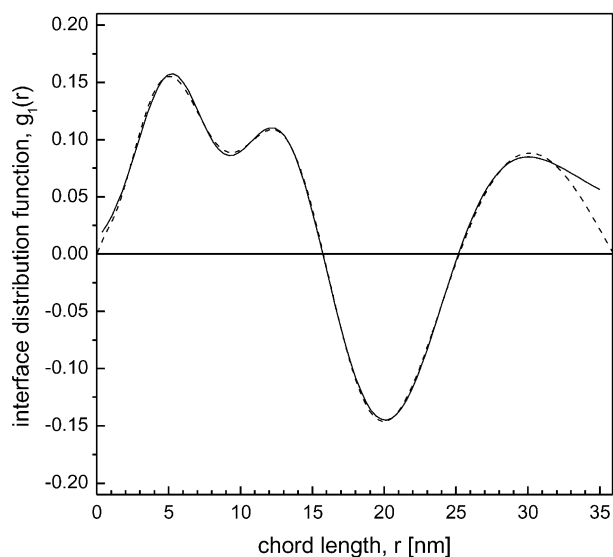


Fig. 5. Experimental interface distribution function $g_1(r)$ of **S2** (solid line) and fit of the data (dashed line) with a situation of a perfect lamellar order but a fluctuating phase thickness with a gaussian distribution of fluctuations.

are in agreement with the structure of undulated lamellae where the one-dimensional undulations are localized in a distorted hexagonal lattice as depicted in Chart 3. The distance between the cylindrical undulations and the intersheet distance were calculated to be 20 and 17 nm, respectively.

The existence of localized undulations was already described in polyelectrolyte–lipid [33,34] and polyelectrolyte–surfactant complexes [35,36]. In those cases (like for the macroscopic counterparts of corrugated cardboard or iron), the localized undulations lead to a remarkable

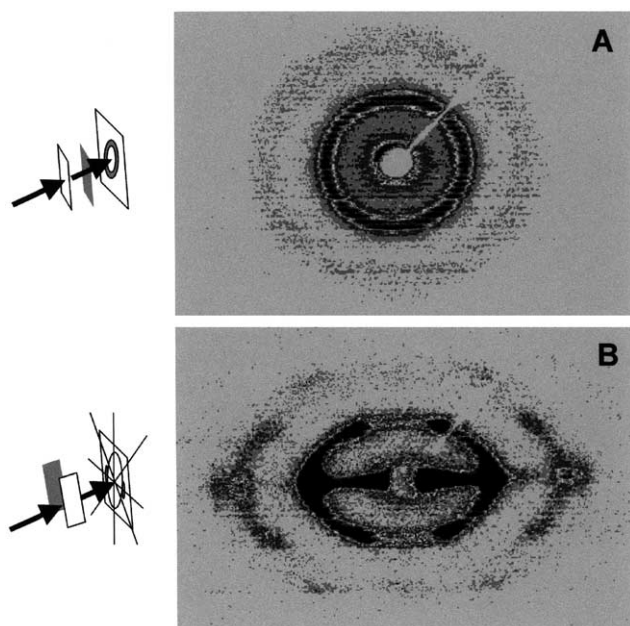


Fig. 6. 2D-SAXS diffractograms of the polymer film of **S4** obtained for orthogonal (A) and parallel (B) alignment of the specimen to the X-ray beam (the radial-averaged SAXS curve of diffractogram A is shown in Fig. 2(B)).

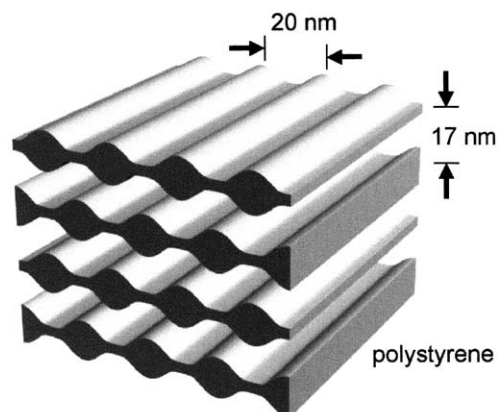


Chart 3. Schematic representation of the *undulated lamellar* morphology of the polymer film **S4**. Note that this structure can be transformed into the zigzag morphology described in Refs. [12,13].

stiffening of the lamellae and a coupled increase of the long-range order. For **S4**, the increase of local order could be visualized by electron microscopy (see Fig. 7). Although affected by the typical defects of self-assembled mesophases, this film shows an extremely long persistence length or stiffness: over the observed area of $2 \times 2 \mu\text{m}^2$, there is practically no tilt of domain orientation. However, we were not able to observe undulations directly (due to problems with the specimen thickness and projection averaging) but the slightly rough structure of those lamellae is clearly visualized.

4. Conclusions

Within the covered range of molecular weights, compositions, and architectures, we were able to repeat and expand previous experiments which showed the

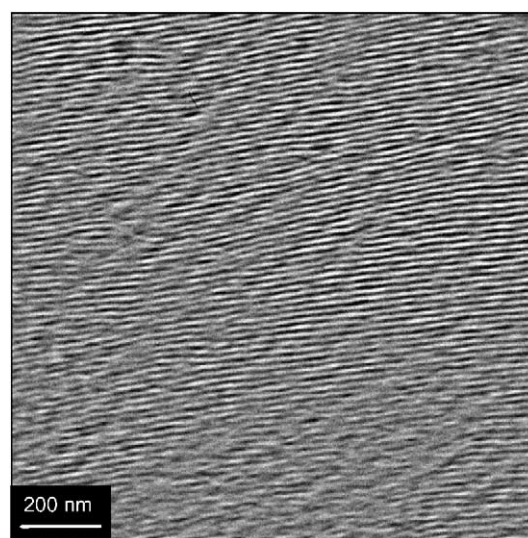


Fig. 7. TEM micrograph of the undulated lamellar morphology of the polymer film **S4**, microtomed perpendicular to the film surface. Note that polypeptide regions appear black due to staining with RuO_4 .

dominance of lamellar morphologies for polystyrene–poly(Z-L-lysine) block copolymer films. In the case of the linear diblock copolymers, refined evaluation techniques on obtained X-ray scattering data showed that all structures are undulated lamellar structures, with the disorder mainly coming from a fluctuating thickness of individual lamellae. Calculation of a geometric interface area factor resulted in values of $\gamma = 1.9$ – 2.6 , showing that the helices are either interdigitated or folded. Both arrangements are able to compensate for the high dipole moment, which is built up along a polypeptide helix.

The bottlebrush-like polymers also form lamellar mesophases, where the bottlebrushes are stacked and form a bilayer-type arrangement. Here, the interface area per polymer chain is significantly larger, and the potential excess area and packing frustrations are compensated for in the structure via the formation of pronounced undulations. For one polymer case, it was shown that those undulations are not necessarily disordered, but can arrange in a deformed hexagonal lattice along the layers, forming a regular corrugated phase.

Future work in this project will focus on how a better long-range ordering of the structures can be achieved, e.g. by applying electrical or magnetic fields or oscillating shear. The characterization of the phase morphologies will be extended, in particular to TEM analyses on polymer films microtomed in different directions, to gain deeper insight into structural details. Furthermore, the influence of other amino acids and sequences shall be used to examine the formation of polymer secondary structures and the development of further tertiary mesophase architectures.

Acknowledgments

We gratefully thank Ines Below, Dr Christian Burger, Jacqueline Conradie-Faul, Dr Charl F.J. Faul, Dr Jürgen Hartmann, Rona Pitschke, and Ingrid Zenke for their valuable contributions to this work. Financial support was given by the Max-Planck-Gesellschaft and the Deutsche Forschungsgemeinschaft (Sfb 448: 'Mesoskopisch strukturierte Verbundsysteme', <http://www.tu-berlin.de/~sfb448/>).

References

- [1] Förster S, Antonietti M. *Adv Mater* 1998;10:195.
- [2] Bates FS, Fredrickson GH. *Phys Today* 1999;52(2):32.
- [3] Bates FS, Fredrickson GH. *Annu Rev Phys Chem* 1990;41:525.
- [4] Matsen MW, Bates FS. *Macromolecules* 1996;29:7641.
- [5] Burger C, Micha MA, Oestreich S, Förster S, Antonietti M. *Europhys Lett* 1998;42:425.
- [6] Klok H-A, Lecommandoux S. *Adv Mater* 2001;13:1217.
- [7] Lee M, Cho B-K, Zin W-C. *Chem Rev* 2001;101:3869.
- [8] Zhong XF, François B. *Makromol Chem, Rapid Commun* 1988;9:411.
- [9] Zhong XF, François B. *Makromol Chem* 1991;192:2277.
- [10] Widawski G, Rawiso M, François B. *Nature* 1994;369:387.
- [11] François B, Pitois O, François J. *Adv Mater* 1995;7:1041.
- [12] Chen JT, Thomas EL, Ober CK, Hwang SS. *Macromolecules* 1995;28:1688.
- [13] Chen JT, Thomas EL, Ober CK, Mao G-P. *Science* 1996;273:343.
- [14] Gallot B. *Prog Polym Sci* 1996;21:1035.
- [15] Deming TJ. *Adv Mater* 1997;9:299.
- [16] Billot J-P, Douy A, Gallot B. *Makromol Chem* 1976;177:1889.
- [17] Perly B, Douy A, Gallot B. *Makromol Chem* 1976;177:2569.
- [18] Billot J-P, Douy A, Gallot B. *Makromol Chem* 1977;178:1641.
- [19] Douy A, Gallot B. *Polymer* 1982;23:1039.
- [20] Janssen K, van Beylen M, Samyn C. *Makromol Chem* 1990;191:2777.
- [21] Yoda R, Hirokawa Y, Hayashi T. *Eur Polym J* 1994;30:1397.
- [22] Micha MA, Burger C, Antonietti M. *Macromolecules* 1998;31:5930.
- [23] Wintermantel M, Gerle M, Fischer K, Schmidt M, Wataoka I, Urakawa H, Kajiwara K, Tsukahara Y. *Macromolecules* 1996;29:978.
- [24] Sheiko SS, Gerle M, Fischer K, Schmidt M, Möller M. *Langmuir* 1997;13:5368.
- [25] Terao K, Takeo Y, Tazaki M, Nakamura Y, Norisuye T. *Polym J* 1999;31:193.
- [26] Kukula H. PhD Thesis. Germany: University of Potsdam; 2001.
- [27] Kukula H, Schlaad H, Tauer K. *Macromolecules* 2002;35:2538.
- [28] Greenfield N, Fasman GD. *Biochemistry* 1969;8:4108.
- [29] Scherrer P. *Gött Nachr* 1918;2:98.
- [30] Klug HP, Alexander LE. *X-ray diffraction procedures for polycrystalline and amorphous materials*. New York: Wiley; 1974.
- [31] Ruland W. *Colloid Polym Sci* 1977;255:417.
- [32] Kricheldorf HR. *α -aminoacid-N-carboxyanhydrides and related heterocycles*. Berlin: Springer; 1987.
- [33] Antonietti M, Kaul A, Thünemann A. *Langmuir* 1995;11:2633.
- [34] Antonietti M, Wenzel A, Thünemann AF. *Langmuir* 1996;12:2111.
- [35] Antonietti M, Burger C, Conrad J, Kaul A. *Macromol Symp* 1996;106:1.
- [36] Antonietti M, Maskos M. *Macromolecules* 1996;29:4199.
- [37] Méring J, Tchoubar D. *J Appl Crystallogr* 1968;1:153.
- [38] Perret R, Ruland W. *J Appl Crystallogr* 1970;3:525.
- [39] Torquato S, Lu B. *Phys Rev E* 1993;47:2950.